Impact Energy Absorption of Concentric Circular Tubes

LION KOK HAO, AMIR RADZI ABDUL GHANI, PRASETYO EDI, KHAIRI YUSUF
Department of Engineering Design & Manufacture,
Faculty of Engineering, University of Malaya,
50603 Kuala Lumpur,
MALAYSIA
amir_radzi@um.edu.my http://design-manufacturer.eng.um.edu.my/

Abstract: - Non-linear finite element code ABAQUS/Explicit was employed to evaluate the energy absorption characteristics of concentric circular tubes subjected to impact in the axial direction. Thin-walled circular tube plays a vital role as energy absorber due to its high energy absorption capacity. However, the main drawback of existing tube type energy absorber is the high initial peak load. This work evaluates the capability of concentric circular tubes in reducing the peak load that is exerted to the protected structures and occupants during impact. Clearance and thickness of the structure were varied and different materials such as aluminum alloy, high strength steel and stainless steel were used. The study found that aluminum alloy has great potential to be utilized as energy absorbing system due to its high specific energy absorption capacity and long stroke. For all materials, increasing the clearance between the inner and outer circular tubes resulted in a reduction of peak load and a significant increase of specific energy absorption (SEA). However, increasing the thickness adversely increased the initial peak load and reduced the SEA. It can be deduced that concentric circular tubes could be utilized as a safer design of energy absorber as it exhibited a lower initial peak load during impact which is a desirable feature when designing for occupant safety.

Key-Words: - structural crashworthiness, impact energy absorption, non-linear explicit finite element

1 Introduction

The field of structural crashworthiness has been developing at a fast pace over the past several decades. Rapid development in this critical field has accelerated design and development of energy absorbers. Energy absorber is a device that functions by absorbing kinetic energy upon impact and dissipating it into other forms of energy, ideally in an irreversible manner [1]. A quality energy absorber should be designed to dissipate the impact energy irreversibly through plastic deformation of metallic structure. Most of the energy absorbers were developed using metallic thin-walled structure as they tends to deform plastically due to elastic-plastic behavior.

Energy absorber plays an important role in various industries ranging from automobile, locomotive, aerospace to naval industries. In automobile industry, the crashworthiness aspect of vehicle design is given top priority. It is due to the high occurrence of accident which always cause casualties and fatalities. The energy absorber can be utilized into upper and lower rails of vehicle frontal structure and car door reinforcement to encounter the side impact event [2]. In the land transportation, highway users are being protected through the advent of W-beam guard rail system and motorway attenuation system. These safety features have high energy absorption characteristics that can decelerate a vehicle to a safe stop even under the condition of a head on crash. Furthermore, an effective energy absorber can also be utilized in the packaging industries. Sensitive goods such electronic devices are protected from damage due to shock loading during transportation or storage. One of the commonly used energy absorber system in packaging industry is the usage of cellulose wadding and foam to provide cushioning effect to the product.

2 Backgrounds

2.1 Literature Review

Energy absorber with circular profile is a popular choice in design and development of energy absorbing system due to its unique characteristics. Previous researches revealed that circular tube has high energy absorption capacity, able to produce reasonably constant operating force and features a high stroke length per unit mass [3]. However, conventional metallic tube type energy absorber resulted in high peak force which may cause serious damages to the protected structures and serious

injuries to the occupants. It is therefore worthwhile to investigate the potential of concentric circular tubes as an alternative solution to minimize the peak force and attain higher specific energy absorption capacity.

Zhang and Cheng [4] carried out comparative studies of energy absorption characteristics of foam filled and multi cell column. Both foam filled and multi cell columns exhibited higher energy absorption as compared to plain columns. In the foam filled column, foam filler acted as a semi-elastic foundation for the sidewall which resulted in decreasing buckling length of sidewall and thus higher plastic deformations and buckling load. In the multi-cell column, the additional bending and stretching of inner cell faces plus the main four faces contribute to the increase of energy absorption. However, the additional stiffness resulted in a high initial peak load which can cause destructive effect on the occupants. The incorporation of a trigger mechanism by means of a groove managed to reduce the high initial peak load while maintaining the energy absorption performance.

Recently, a novel idea of installing a buckling initiator near the impact end of an axially crushed square tube was proposed [5]. The buckling initiator composed of a pre-hit column and pulling strips. It succeeded in reducing the initial peak force of the square tubes while retaining its progressive deformation mode and favourable energy absorption capability.

2.2 Characteristics of Energy Absorber

The capability of an energy absorber in dissipating the impact energy depends on the extent of plastic deformation behavior of the metallic structures. Since metallic structure exhibit the ductile behavior upon impact loading, it is widely utilized as a popular material in design and development of energy absorber. Stroke length of energy absorber should be sufficient to absorb a large amount of impact energy. Long stroke along with a restricted and almost constant reactive force promised a higher absorbed energy. It is due to the fact that energy absorbed is equal to its magnitude times the displacement experienced along the acting line of the force.

One of the main aims of energy absorber is to minimize the damages or injuries to the protected object. Hence, the kinetic energy should be dissipated with a longer time. The longer time that force prevails, the gentler is the arresting force required and the smaller is the injury sustained. The device should be designed to deform with good stability and repeatability, so as to ensure the reliability of the structure in its service. Phenomenon like catastrophic failure and Euler buckling should be avoided as these collapse modes affect the energy absorption efficiency of the structure significantly.

Light weight property should be embarked into the material selection for a quality energy absorber. It is because an increase in weight implies more consumption of fuel and more pollution of the environment. Recently, space frame design of car body using aluminum alloy demonstrated the commitment of automobile maker to design a quality energy absorber by not neglecting the environmental issues. Fabrication cost of energy absorber should be minimised. Energy absorber is a one shot item which means having once been deformed, they are discarded and replaced. Hence, the economical aspect of this device should be taken into consideration so that the society can really benefits from the invention of an efficient and cost effective energy absorber.

Energy absorption characteristics of concentric circular tubes are quantified in terms of specific energy absorption (SEA) and crush force efficiency (CFE). Specific energy absorption is defined as the energy absorbed by the tube divided by the mass of the tube. Ratio of mean load to peak load is called the crush force efficiency (CFE) and it is used to define the performance of the structure during impact. Al Galib, D. [6] stated that the initial peak load in force-displacement curve is always higher than the subsequent peak load. Initially, the structure is free of deformation and hence higher load is required to initiate the deformation stage. (See Figure 1). Deformation formed during this fold is going to influence the formation of the next one by producing a local bending at the plastic hinges level. This phenomenon caused the subsequent peak load to be reduced. The ideal energy absorber demonstrates a long, flat force-displacement curve (See Figure 2). An efficient energy absorber should be designed with the longest plateau force. Harte, A. M. [7] recommended that the selection of plateau force should not cause any damage to the protected object.

$$SEA = \frac{E_{abs}}{m}, \quad (1)$$

where, E_{abs} is the energy absorbed and m is the mass of tubes.

$$CFE = \frac{F_{av}}{F_{\max}} \quad (2)$$

where F_{av} is the mean force and F_{max} is the initial peak force.

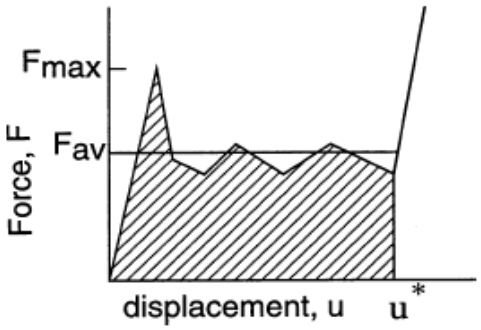

Figure 1: The force-displacement curve of a practical energy absorber [7]

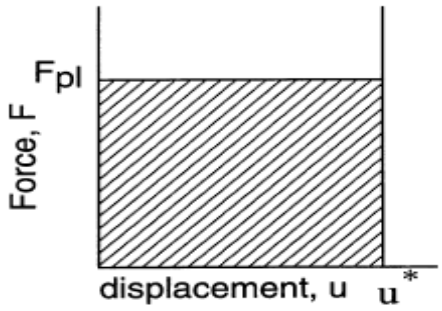

Figure X: The force-displacement curve of an ideal energy absorber [7]

The aim of this study is to quantify the energy absorption characteristics of concentric circular tubes under axial impact loading and investigate the influence of tube thickness and clearance between the inner and outer tubes, and different materials on the energy absorption efficiency. Clearance and thickness were varied to establish a relationship between the energy absorption characteristics with the geometrical configurations of the structure.

3 Finite Element Modelling

Dynamic load is defined as the load which is applied at a high rate and associated with large plastic strain that dominates over the elastic strain. Finite element analysis (FEA) is increasingly popular in design, analysis and optimization of energy absorber. This method is capable of assessing the crashworthiness aspect of a structural component with less time and lower cost as compared to experimental based approaches. Numerical simulation of axial crushing of circular tubes was conducted using ABAQUS/Explicit. Preliminary result of an axially crushed aluminium tube subjected to impact mass of 500 kg and impact speed of 10 m/s was found to be in good agreement with the experimental results from Gameiro, C.P. et al [8], thus demonstrating the confidence, reliability and accuracy of the FEA technique (See Figures 3 and 4). Therefore, further exploration of the energy absorbing characteristics of the concentric tubes was carried out employing this method.

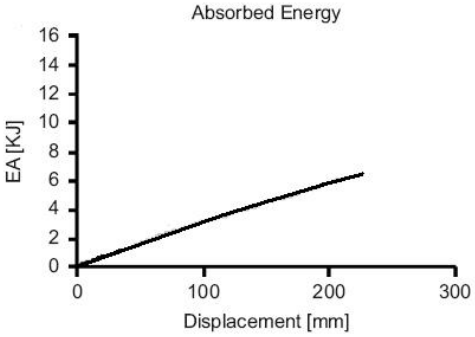

Figure 3: Absorbed energy curve from experimental method (C.P Gameiro et al [8])

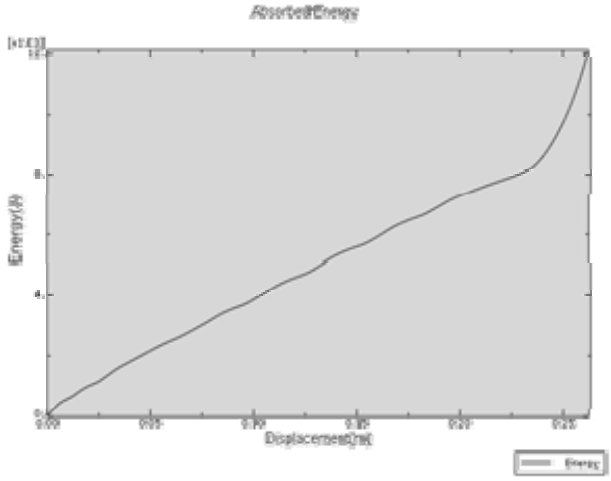

Figure 4: Absorbed energy curve from numerical simulation

The tubes were modeled in Abaqus as a 3D deformable shell. The bottom plate which represented the support and the top plate which represented the impactor were modeled as discrete rigid bodies. Figure 5 shows the assembled finite element model. A global seed length of 3 mm was used and a total of 2500 to 3000 linear quadrilateral explicit shell element of type S4R was created for

the tubes. For the two rigid bodies, a total of 1800 to 2000 linear quadrilateral elements of type R3D4 were created. Concentric tubes parameters and dimensions are given in Figure 6 and Table 1. The tubes overall length were fixed at 180 mm.

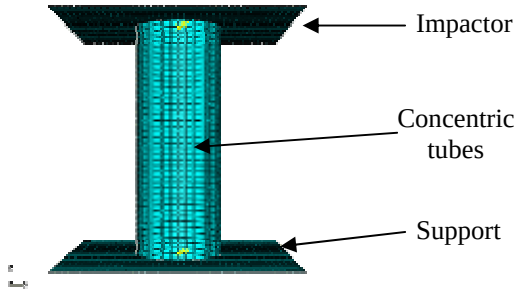

Figure 5 : Assembly of Finite Element Models

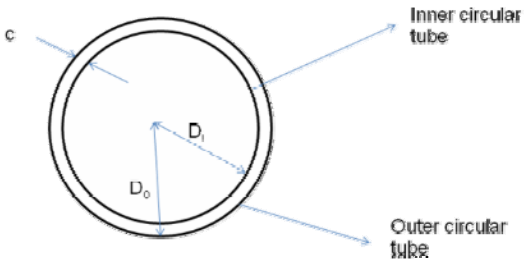

Figure 6 : Concentric Tubes Parameters

Table 1 : Dimension of Concentric Tubes With Varying Clearance

Inner Tube Diameter, D_i (mm)	Outer Tube Diameter, D_o (mm)	Clearance, c (mm)
64.96	76	8
54.96	76	18
44.96	76	28
34.96	76	38

Table 2 : Dimension of Concentric Tubes With Varying Thickness with Clearance of 10 mm

Inner Tube Diameter, D_i (mm)	Outer Tube Diameter, D_o (mm)	Clearance, c (mm)
63.2	76	1.4
62.8	76	1.6
62.4	76	1.8
62.0	76	2.0

Material properties assigned to the model followed the material relationship of elastic-plastic linear strain hardening with rate dependence. Table 3 shows the mechanical properties of the selected materials. Table 4 shows the Cowper Symonds constants for the selected materials.

Table 3 : Mechanical Properties of Selected Materials [9]

	Alum 2014-T6	SSAB Tunnplat Docol 1000 DP High Strength Steel	Industeel URANUS 45N+22%Cr Austenitic-Ferritic Duplex Stainless Steel
Density (kg/m^3)	2800	7870	7800
Yield strength (MPa)	414	950	510
Ultimate tensile (UTS) (MPa)	483	1200	720
Young's Modulus (GPa)	73.1	207	200
Poisson's Ratio	0.3	0.3	0.3
Plastic strain at UTS	0.23	0.2	0.3

Table 4 : Cowper Symonds Constants [10]

Material	D(s^{-1})	q
Aluminum 2014-T6	6500	4
SSAB Tunnplat Docol 1000 DP High Strength Steel	40.4	5
Industeel URANUS 45N+22% Cr Austenitic-Ferritic Duplex Stainless Steel	100	10

A dynamic explicit solver Abaqus Explicit which is most suited to carry out non-linear, low to high speed impact analysis was chosen. Time duration of 0.02 s was specified. The contact behavior between the tubes, support and impactor during collision was set up under the interaction module. The contact property consisted of tangential behavior, which used a 'penalty' friction formulation with a coefficient of 0.25 to prevent sliding of the tubes at the support end. The normal behavior used the 'hard contact' formulation to allow separation after contact. A general dynamic (explicit) contact was utilized where all the contact surfaces are automatically identified by the system.

Boundary conditions and impact speeds were specified in the load module. For the impactor, the boundary conditions were V1=V3=VR1=VR2 = VR3, which implies that it could only move in the vertical z-direction. The support was fully constrained. The bottom edges of the tubes were constrained in the z-direction only. Movement in the x- and y-direction was restrained by the friction between the tubes and the support. Impactor velocity of 10 m/s was specified in the predefined field and the impactor mass of 250 kg was inputed as inertia in the engineering features.

4 Results and Discussion

Force-displacement curve is a useful tool to evaluate the energy absorption efficiency of an energy absorber. It enables us to determine the peak load, the mean load and the crushing distance of the structure. Typical force displacement curve of crashworthy structure always showed high initial peak load followed by oscillations. The peak load corresponds to the formation of inward or outward parts of the folds.

4.1 Effect of Clearance

Figure 7 shows the force-displacement plots of aluminium alloy with varying clearances. Figure 8 shows the force-displacement plots of high strength steel with varying clearances. Both materials exhibited high initial peak loads followed by much lower and constant mean loads. For aluminium alloy, the sudden increase in load towards the end of the crush travel indicated that the material has fully crushed and the impactor was transmitting the force directly to the support. For both materials, increasing the clearance reduced the initial peak loads. For aluminium alloy, tubes with clearances of 8 mm and 18 mm showed little difference in initial peak loads and mean loads. Increasing further the clearance to 28 mm and 38 mm resulted in small drop in peak loads and substantial drop in mean loads. Reduction of initial peak loads and mean loads with the increase of clearance were more gradual for the high strength steel.

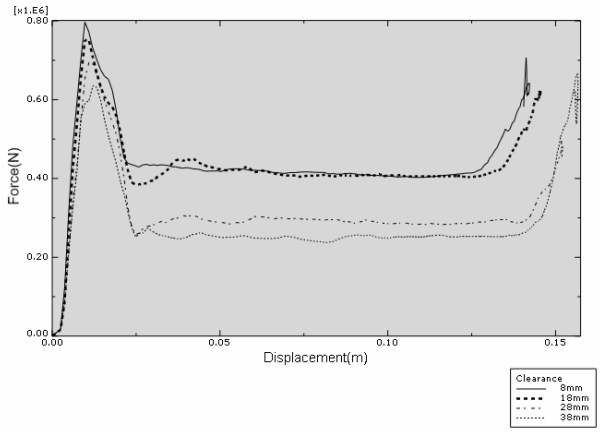

Figure 7 : Force-displacement Plots for Aluminium Alloy with Varying Clearances

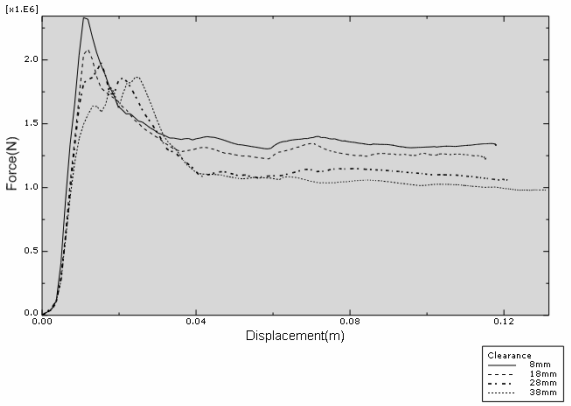

Figure 8 : Force-displacement Plots for High Strength Steel with Varying Clearances

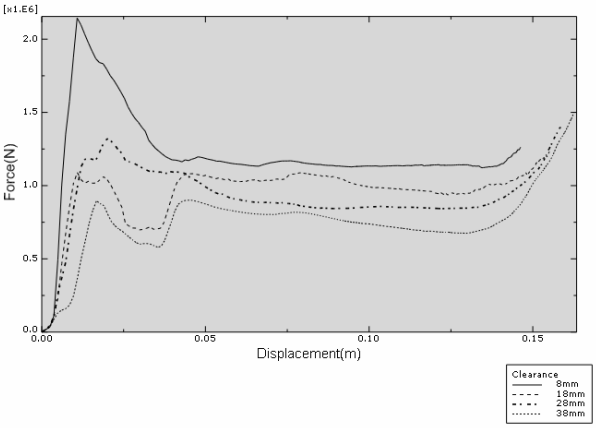

Figure 9 : Force-displacement Plots for Stainless Steel with Varying Clearances

Figure 9 shows the force-displacement plots of stainless steel with varying clearances. Stainless steel with clearance of 8 mm exhibited the highest initial peak loads. Increasing the clearance seemed to greatly reduce the initial peak loads with the 18 mm clearance showing the almost ideal characteristic of the constant mean load with minimal initial peak load. However, further increasing the clearance tended to cause reduction in mean load during the initial crushing of the tubes before the sudden increase at crushing distance of 50 mm.

Figure 10 and 11 shows the graphs of mean load against clearance and peak loads against clearance for the various materials. It can be seen that all materials exhibited lower mean loads and peak loads as clearances were increased. Stainless steel exhibited a substantial drop in initial peak load at clearance of 18 mm before gradually increasing at

higher clearances but the values were still very much below the initial peak load at clearance of 8 mm. Figure 12 shows the graph of crush force efficiency against clearance for various materials. High strength steel tended to exhibit constant crush force efficiency over a range of clearance. Aluminium alloy showed constant crush force efficiency until clearance of 18 mm before gradually reducing at higher clearances. Stainless steel on the hand displayed an increase of crush force efficiency at clearance of 18 mm before substantially reducing at higher clearances.

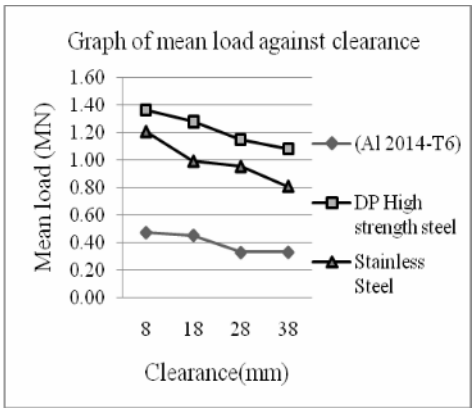

Figure 10 : Graph of Mean Load against Clearance for Various Materials

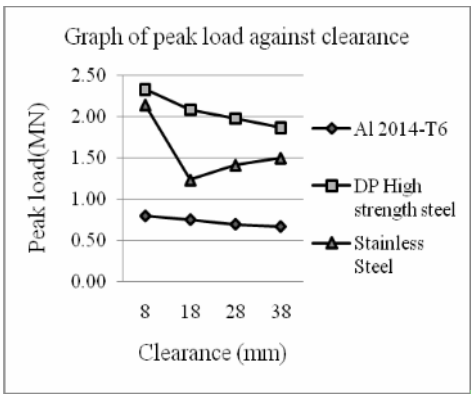

Figure 11 : Graph of Peak Load against Clearance for Various Materials

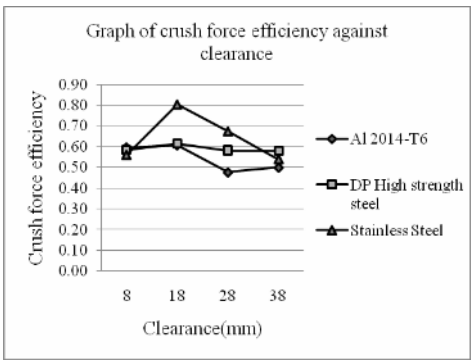

Figure 12 : Graph of Crush Force Efficiency against Clearance for Various Materials

Figure 13 shows the graph of specific energy absorption (SEA) against clearance. All materials exhibited gradual increase in SEA with the increase of clearance. Due to its lower density, aluminium alloy has the highest SEA which would make it the most attractive option for automotive application. The high strength steel and stainless steel have almost similiar SEA.

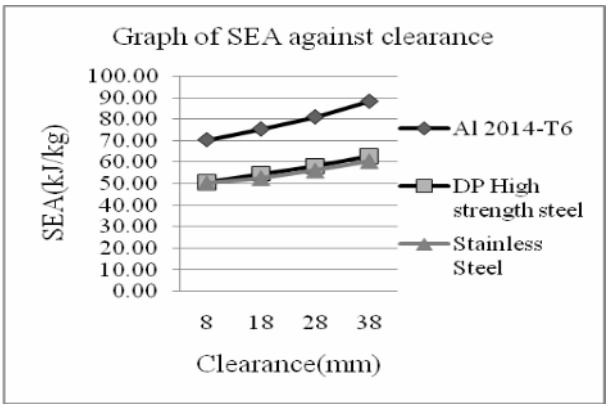

Figure 13 : Graph of Specific Energy Absorption (SEA) against Clearance for Various Materials

Figure 14 shows the deformed shapes of aluminium alloy concentric tubes with clearances of 8 mm and 38 mm respectively. Both tubes exhibited progressive failure mode with diamond pattern. For the tubes with 38 mm, it can be observed that the outer tube failed in a three sided (triangular) diamond pattern while the much smaller inner tube failed in a two sided (oblong) diamond pattern. Figure 15 shows the deformed shapes of high strength steel concentric tubes with clearances of 8 mm and 38 mm. Concentric tubes with 8 mm clearance exhibited uniform diamond mode progressive failure while concentric tubes with 38 mm clearance showed a mixture of concertina and diamond modes progressive failure and a small amount of Euler buckling which can lead to instability. Figure 16 shows the deformed shapes of stainless steel concentric tubes with clearances of 8 mm and 38 mm. Concentric tubes with clearance of 8 mm exhibited an almost perfect diamond mode progressive failure with uniform folding for both the outer and inner tubes. Concentric tubes with clearance of 38 mm displayed a combination of diamond and concertina modes progressive failures with a small amount of Euler buckling. Concertina mode occurred at the ends of the tubes while the diamond mode was more prevalent in the middle portion of the tubes.

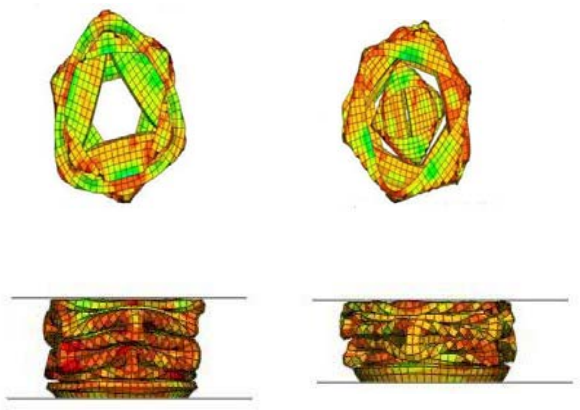

(a) (b)

Figure 14: Final deformed shapes of aluminium alloy concentric tubes with clearances of (a) 8 mm and (b) 38 mm

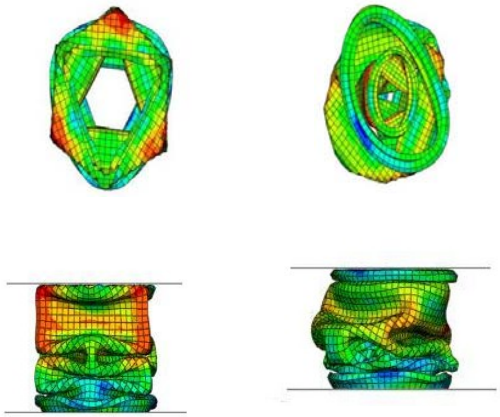

(a) (b)

Figure 15: Final deformed shapes of high strength steel concentric tubes with clearances of (a) 8 mm and (b) 38 mm

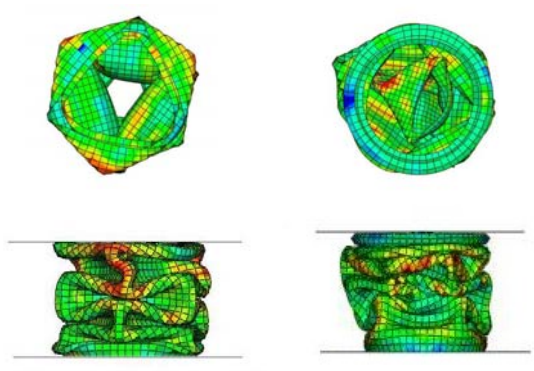

(a) (b)

Figure 16: Final deformed shapes of stainless steel concentric tubes with clearances of (a) 8 mm and (b) 38 mm

4.2 Effect of Tube Thickness

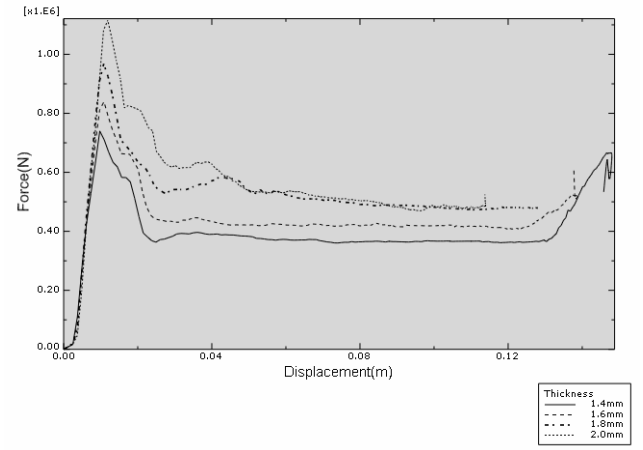

Figure 17 : Force-displacement Plots for Aluminium Alloy with Varying Thicknesses

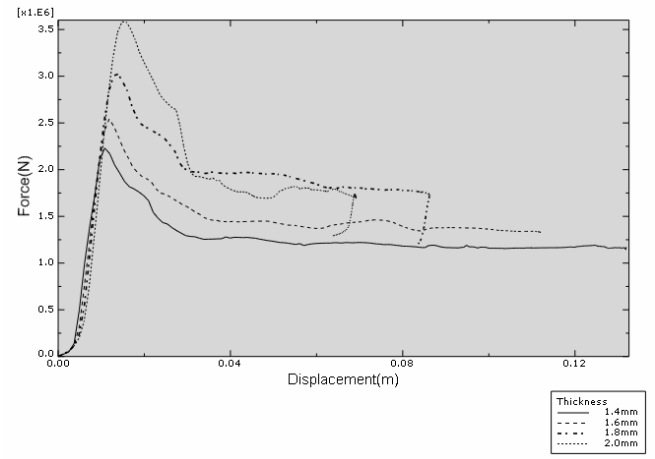

Figure 18 : Force-displacement Plots for High Strength Steel with Varying Thicknesses

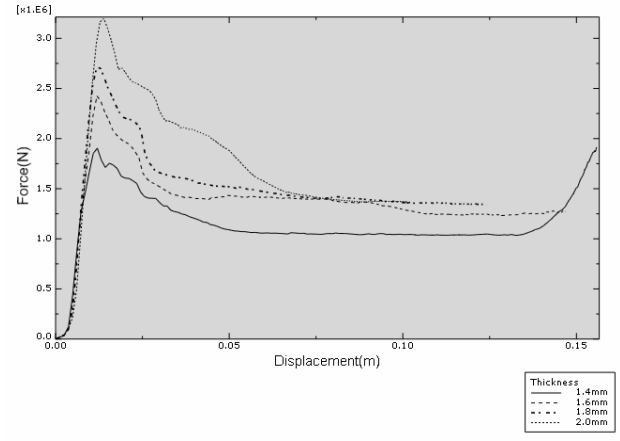

Figure 19 : Force-displacement Plots for Stainless Steel with Varying Thicknesses

Figures 17, 18 and 19 show the force-displacement plots with varying thicknesses for aluminium alloy, high strength steel and stainless steel respectively. It can be seen that for all materials, increase in thickness resulted in increase in initial peak loads and mean loads. However, the increase in peak loads was more substantial as compared to increase in mean loads which will have an adverse effect on the CFE. Also, increase in thickness resulted in reduction of crushing length.

For aluminium alloy, tube thicknesses of 1.8 mm and 2 mm seemed to produce equal mean loads but different initial peak loads with the 2 mm thickness having a slightly shorter crushing distance. High strength steel with tube thicknesses of 1.8 mm and 2 mm also seemed to exhibit similiar mean loads but different peak loads. For stainless steel, the effect of thickness on mean load was not so prominent as tube thickness of 1.6 mm to 2 mm gave similiar mean loads even though the peak loads were different.

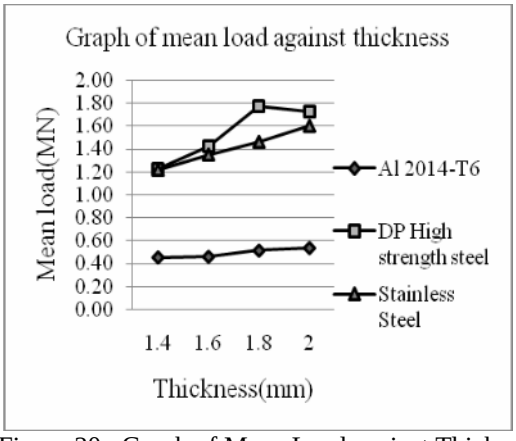

Figure 20 : Graph of Mean Load against Thickness for Various Materials

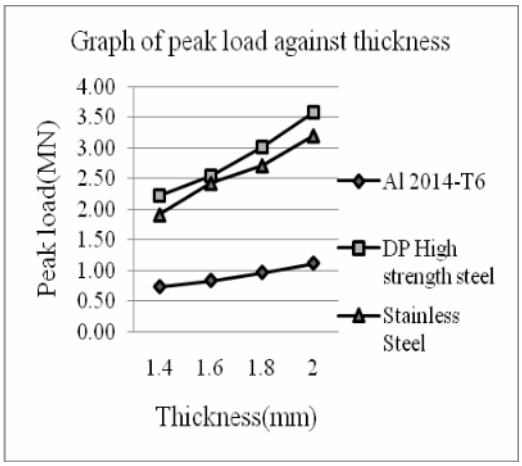

Figure 21 : Graph of Peak Load against Thickness for Various Materials

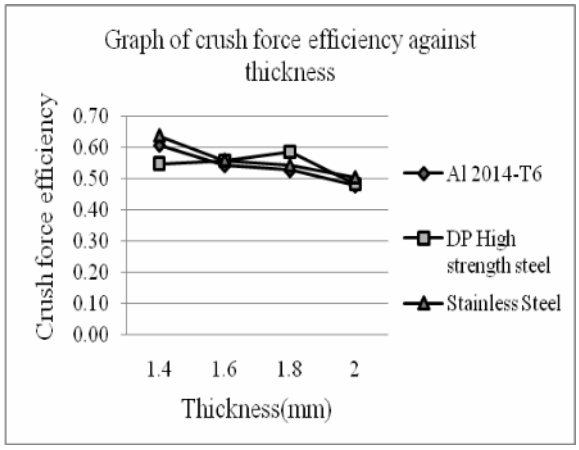

Figure 22 : Graph of Crush Force Efficiency against Thickness for Various Materials

Figures 20, 21 and 22 show the graphs of mean load, peak load and crush force efficiency against thickness respectively for all materials. Both stainless steel and high strength steel showed a gradual increase in mean loads. However, aluminium alloy exhibited a rather drastic increase in mean load until a thickness of 1.8 mm before gradually dropping to slightly lower value. All materials showed an increase of peak loads with the increase of thickness. Aluminium alloy exhibited a more gradual increase in peak loads as compared to the high strength steel and stainless steel. Stainless steel and aluminium alloy showed gradual decrease in CFE. High strength steel showed a gradual increase in CFE until thickness of 1.8 mm before gradually dropping at 2 mm thickness.

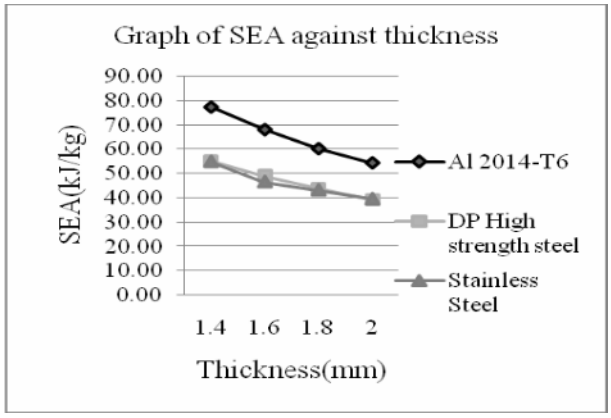

Figure 23 : Graph of SEA against Thickness for Various Materials

Figure 23 shows the graph of specific energy absorption (SEA) against thickness. All materials showed a decrease in SEA with the increase of tubes thicknesses. Due to its lower density, aluminium alloy has the highest SEA. Both high strength steel and stainless steel have similar SEA.

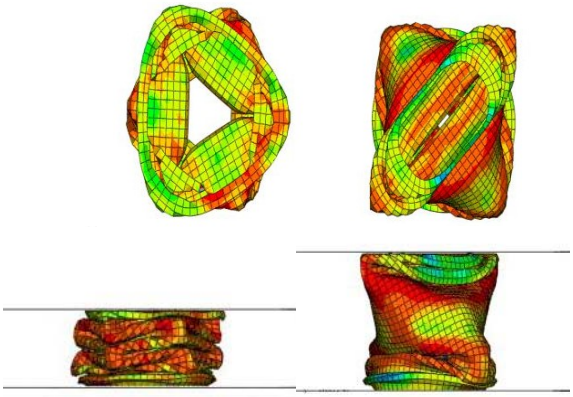

(a) (b)

Figure 24: Final deformed shapes of aluminium alloy concentric tubes with thicknesses of (a) 1.4 mm and (b) 2 mm

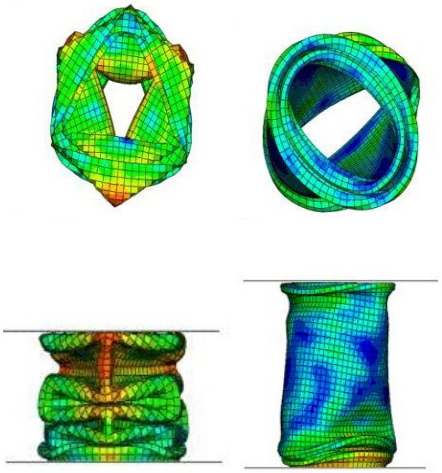

(a) (b)

Figure 25: Final deformed shapes of high strength steel concentric tubes with thicknesses of (a) 1.4 mm and (b) 2 mm

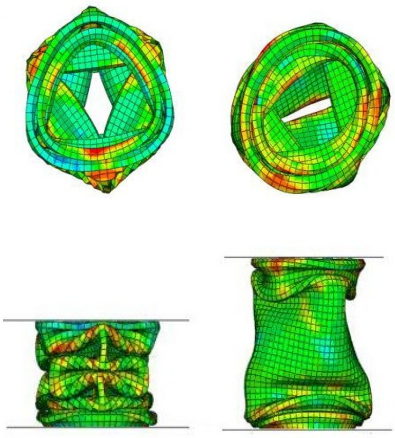

(a) (b)

Figure 26: Final deformed shapes of stainless steel concentric tubes with thicknesses of (a) 1.4 mm and (b) 2 mm

Figure 24 shows the deformed shapes of aluminium alloy concentric tubes with thicknesses of 1.4 mm and 2 mm respectively. Tubes with thickness of 1.4 mm deformed in a diamond pattern progressive failure mode while tubes with 2 mm thickness exhibited a mixture of concertina and Euler buckling modes. Figure 25 shows the deformed shapes of high strength steel concentric tubes with thicknesses of 1.4 mm and 2 mm respectively. Tubes with thickness of 1.4 mm showed an almost perfect diamond pattern failure mode. Both inner and outer tubes failed in a three sided diamond shape. Tubes with 2 mm thickness failed in a concertina mode at the two ends followed by an Euler buckling mode in the middle portion. Figure 26 shows the deformed shapes of stainless steel concentric tubes with thicknesses of 1.4 mm and 2 mm respectively. Tubes with 1.4 mm thickness failed in a uniform diamond pattern failure mode. Tubes with 2 mm thickness exhibited a mixture of concertina and Euler bucking failure modes. Euler buckling modes seemed to be more prominent in both the aluminium alloy and stainless steel tube with 2 mm thickness as compared to the high strength steel. These less than ideal failure modes resulted in lower SEA for all tubes with thickness of 2 mm.

5 Conclusions

Increasing the clearance between inner and outer circular tubes from 8 mm to 38 mm resulted in the decrease of the peak loads and mean loads for all materials. However, CFE was more or less constant for the aluminium alloy. For the high strength steel, the CFE was constant until 18 mm clearance before gradually decreasing at higher clearances. For stainless steel, the CFE increased significantly until clearance of 18 mm before gradually decreasing at higher clearances. For all materials, increased in clearance resulted in increase in SEA.

Increasing the thickness of the tubes from 1.4 mm to 2 mm resulted in the increase of peak loads and mean loads. The increase was more prominent for the high strength steel and stainless steel as compared to the aluminium alloy. The CFE showed a decrease for aluminium alloy and stainless steel with increased thickness. High strength steel exhibited a gradual increase of CFE until thickness of 1.8 mm before gradually decreasing. The SEA showed a decrease for all materials.

Size of the clearance between inner and outer circular tubes, thickness of tubes and type of

materials influenced the collapse mode of the concentric tubes. Collapse modes were mainly concertina and diamond mode progressive failures. A combination of concertina, diamond and small amount of Euler buckling was observed for concentric tubes with larger clearances and thicknesses and stiffer materials such as stainless steel and high strength steel.

This work demonstrates the possibilities of modifying the structure impact energy absorption characteristics by the variation of clearances between the concentric tubes, thickness of tubes and materials. It is believed that it is possible to tailor the structure performance over a wide range of conditions by the use of this method. Therefore, a more detailed and systematic investigation on other parameters such as the different thickness of inner and outer tubes, coefficient of friction between inner and outer tubes and addition of different fillers between the tubes will be carried out in the near future.

References:

[1] Olabi, A.G, Morris, E and Hashimi, M.S.J. (2007), "Metallic tube type energy absorbers: A synopsis", Thin-Walled Structure, Vol. 45, pp.706-726.

[2] Yu, T. X. and Lu, G. (2003). Energy absorption of structures and materials, Woodhead Publishing, Cambridge, United Kingdom.

[3] Alghamdi, A.A.A. (2001), "Collapsible impact energy absorbers: an overview", Thin-Walled Structures, Vol.39, pp.189-213.

[4] Zhang, X. and Cheng, G. (2007). A comparative study of energy absorption characteristics of foam filled and multi-cell square column. Int. Journal of Impact Engineeirng. 34: 1739-1752

[5] Zhang, X.W., Su, H. and Yu, T.X. (2009). Energy absorption of an axially crushed square tube with a buckling initiator. International Journal of Impact Engineering. 36: 402-417

[6] Al Galib, D and Limam,A. (2004). Experimental and numerical investigation of static and dynamic axial crushing of circular aluminium tubes. Thin-walled Structures. Vol.42, pp 1103-1137.

[7] Harte, A-M and Fleck, N.A. (2000). Energy absorptions of foam filled circular tubes with braided composite walls. Eur J. Mech. A/ Solids. Vol. 19, pp31-50.

[8] C.P Gameiro and J.Cirne (2007), "Dynamic axial crushing of short to long circular aluminum tubes with agglomerate cork filler", International Journal of Mechanical Sciences Vol.49, pp.1029-1037

[9] www.matweb.com

[10] Jones, N. (1997). Structural Impact, Cambridge University Press.

[11] Abaqus 6.7 User Manuals. (2007). Dassault System.

[12] Prasetyo Edi. A Flow Control for a High Subsonic Regional Aircraft Exploiting a Variable Camber Wing with Hybrid Laminar Flow Control. IASME TRANSACTIONS Journal on Fluid Mechanics and Aerodynamics, Included in ISI/SCI Web of Science and Web of Knowledge, Issue 6, Volume 2, August 2005, ISSN 1790-031X, page 927-936.

[13] Prasetyo Edi. An Aircraft Family Concept for a High Subsonic Regional Aircraft. IASME TRANSACTIONS Journal on Fluid Mechanics and Aerodynamics, Included in ISI/SCI Web of Science and Web of Knowledge, Issue 7, Volume 2, September 2005, ISSN 1790-031X, page 1140-1148.

[14] Prasetyo Edi. The Development of N-250 Military Version. WSEAS TRANSACTIONS on Fluid Mechanics, Included in ISI/SCI Web of Science and Web of Knowledge, Issue 8, Volume 1, August 2006, ISSN 1790-5087, page 832-837.

[15] Prasetyo Edi, Nukman Y. and Aznijar A. Y. The Application of Computational Fluid Dynamic (CFD) on the Design of High Subsonic Wing. WSEAS TRANSACTIONS on APPLIED and THEORETICAL MECHANICS, Included in ISI/SCI Web of Science and Web of Knowledge, Issue 9, Volume 3, September 2008, ISSN : 1991-8747.